

X-RAY ISOPHOTES IN A RAPIDLY ROTATING ELLIPTICAL GALAXY:
EVIDENCE OF INFLOWING GASFABRIZIO BRIGHENTI^{1,2}, WILLIAM G. MATHEWS¹, PHILIP J. HUMPHREY³, DAVID A. BUOTE³*Draft version September 15, 2021*

ABSTRACT

We describe two-dimensional gasdynamical computations of the X-ray emitting gas in the rotating elliptical galaxy NGC 4649 that indicate an inflow of $\sim 1 M_{\odot} \text{ yr}^{-1}$ at every radius. Such a large instantaneous inflow cannot have persisted over a Hubble time. The central constant-entropy temperature peak recently observed in the innermost 150 parsecs is explained by compressive heating as gas flows toward the central massive black hole. Since the cooling time of this gas is only a few million years, NGC 4649 provides the most acutely concentrated known example of the cooling flow problem in which the time-integrated apparent mass that has flowed into the galactic core exceeds the total mass observed there. This paradox can be resolved by intermittent outflows of energy or mass driven by accretion energy released near the black hole. Inflowing gas is also required at intermediate kpc radii to explain the ellipticity of X-ray isophotes due to spin-up by mass ejected by stars that rotate with the galaxy and to explain local density and temperature profiles. We provide evidence that many luminous elliptical galaxies undergo similar inflow spin-up. A small turbulent viscosity is required in NGC 4649 to avoid forming large X-ray luminous disks that are not observed, but the turbulent pressure is small and does not interfere with mass determinations that assume hydrostatic equilibrium.

Subject headings: Cooling flows - galaxies:elliptical and lenticular - galaxies:individual (NGC4649) - galaxies:ISM - galaxies:kinematics and dynamics - X-rays:galaxies

1. INTRODUCTION

X-ray isophotes of massive, rotating elliptical galaxies convey valuable information about the rotation of the hot, virialized interstellar gas, the interaction of this gas with gas recently ejected from evolving stars, and the sense of radial motion – in or out – of the hot gas. These issues are relevant to understanding the physical nature of the hot gas in galaxy groups and clusters in which gas loses energy by radiating X-rays but does not appear to cool to low temperatures as expected. In traditional cooling flows the radiating gas approximately maintains the local virial temperature as it flows slowly toward the center of the confining gravitational potential, then cools catastrophically near the center. The so-called cooling flow problem arises because there is insufficient spectroscopic evidence for cooling gas, previously cooled gas or recently formed stars. This paradox is apparent in massive galaxy clusters, galaxy groups and individual elliptical galaxies, i.e. the cooling flow problem is independent of scale. For this reason observations of X-ray luminous, relatively nearby elliptical galaxies can provide important clues to unravel the mysteries of cooling flows that do not seem to cool.

The recent deep 81ks Chandra observation of the nearby X-ray luminous elliptical galaxy NGC 4649 by Humphrey et al. (2008) led to the detection of a massive central black hole ($M_{bh} = 3 \times 10^9 M_{\odot}$). This super-

massive black hole was found for the first time directly from X-ray data by assuming that the hot gas is very nearly in hydrostatic equilibrium. The increased quality of the X-ray observations of NGC 4649 has motivated us to develop a dynamical model for the hot gas flow in this rotating galaxy.

At any time the radial flow of hot gas must either be inward, outward, a combination of the two, or stationary. Many people think that cooling inflows cannot occur in elliptical galaxies or elsewhere because of the absence of X-ray spectral emission at low and intermediate temperatures (e.g. Xu et al. 2002). We showed for galactic-scale cooling flows that dust expelled from stars can cool the gas so fast that very little low-temperature thermal X-ray emission occurs (Mathews & Brighenti 2003a). Nevertheless, cooling inflows cannot dominate over time since the central mass accumulated would greatly exceed limits set by the velocity dispersion of central stars. Detailed gasdynamical models with *ad hoc* heating sources have shown that the transition from cooling inflows to strong low-density wind outflows is very abrupt (Mathews & Brighenti 2003b). In the absence of extreme fine tuning, most of the X-ray luminous hot gas bound to elliptical galaxies cannot be flowing globally outward, although inhomogeneous outflowing regions of lower gas density (and X-ray emissivity) in jets or buoyant regions are not ruled out. If the gas is not flowing at all, continued enrichment by Type Ia supernovae for a few Gyrs will raise the iron abundance to several times that of the underlying stars, which is not generally observed (e.g. Humphrey & Buote 2006). One way to avoid this enrichment catastrophe is to recognize that some or most of the SNIa iron may cool radiatively in a way that cannot be observed, as discussed by Brighenti & Mathews (2005).

¹ University of California Observatories/Lick Observatory, Department of Astronomy and Astrophysics, University of California, Santa Cruz, CA 95064 mathews@ucolick.org

² Dipartimento di Astronomia, Università di Bologna, via Ranzani 1, Bologna 40127, Italy fabrizio.brighenti@unibo.it

³ Department of Physics and Astronomy, University of California at Irvine, 4129 Frederick Reines Hall, Irvine, CA 92697-4575

However, the modest SNIa enrichment observed in the hot gas can be understood if much of the hot galactic gas flows radially inward, and the abundance can be even further reduced if more extended circumgalactic group-scale gas with relatively low metallicity flows inward past the sources of stellar enrichment. Circumgalactic gas is likely since Humphrey et al. (2006) derive a group-level virial mass for NGC 4649, $3.5 \times 10^{13} M_{\odot}$.

Several additional observations of NGC 4649 can be understood most easily in terms of gaseous inflow. First, the central gas temperature peak discovered by Humphrey et al. (2008) within a few 100 parsecs was predicted by cooling *inflow* models as gas approaches a massive central black hole (Brighenti & Mathews 1999). While only a central gas pressure peak is sufficient to determine the black hole mass, a peak in the gas temperature is a signature of compressional heating as hot gas flows inward toward a strongly concentrated mass or small rotating disk. This compressive heating can occur even when the gas is losing energy by standard radiative losses. Additional support for subsonic compressional heating during inflow follows from the observation that the entropy of hot gas closest to the black hole is lower than in any other region in NGC 4649 so it has not been recently heated by the central AGN.

Another important signature of subsonically inflowing gas seen in NGC 4649 and other similar elliptical galaxies is a central flattening of X-ray isophotes on kpc scales. Elliptical X-ray isophotes on galactic scales have different implications than on larger scales which have been used to infer flattening of the dark halo potential (Buote et al. 2002). Isophotal flattening in excess of that required by the underlying stellar potential can be interpreted as a spinning up of hot inflowing gas expected when angular momentum is exchanged with gas recently ejected from old, mass-losing red giant stars that participate in the galactic rotation. We review below the recent compilation of Chandra isophotes of elliptical galaxies by Diehl & Statler (2007) and show that they generally resemble NGC 4649 in central flattening and implied inflow spin-up. NGC 4649 is an ideal candidate galaxy to study the influence of rotation on the X-ray isophotes because of its remarkably high rotation rate for a massive, cored E galaxy, its proximity, and our good fortune to have received at least one moderately deep Chandra observation.

In the following discussion we review the implications of recent Chandra images of NGC 4649 and present gas-dynamical models of increasing complexity. Unlike our previous studies of rotating cooling flows (Brighenti & Mathews 1996, 2000), we include the important contribution of inflowing and non-rotating circumgalactic gas from a group-scale halo. In addition, since the central X-ray isophotal flattening observed in NGC 4649 and other massive ellipticals is less than that expected from the conservation of angular momentum, we invoke an *ad hoc* hot gas turbulence that can transport angular momentum away from the galactic spin axis. By combining turbulence and circumgalactic inflow it is easy to explain the isophotal flattening observed in NGC 4649. Moreover, the turbulent viscosity that is consistent with the X-ray isophotes of NGC 4649 generates a turbulent pressure that is much less than the gas pressure. Therefore,

the subsonic turbulent activity required to reduce the angular momentum does not significantly degrade the total mass determinations of Humphrey et al. (2008) based on assuming hydrostatic equilibrium. We assume that the mild turbulence we require is produced by energy released near the central black hole or active galactic nucleus (AGN).

Our treatment here is done under the assumption that most of the *observed* X-ray emission in NGC 4649 can be explained with inflowing gas. We do not propose that this is the complete solution to the gas flow problem in this or other similar galaxies, but only demonstrate that the X-ray observations are consistent with an *apparent* global inflow at the present time. To avoid unobserved catastrophic radiative cooling and a huge mass concentration in the galactic core, we must also assume that there is a (possibly buoyant) return mass outflow that is too intermittent, too hot, or too cunningly disguised to contribute to Chandra observations (Mathews & Brighenti 2004; Brighenti & Mathews 2006).

2. STELLAR ROTATION, X-RAY ISOPHOTES AND COOLING INFLOW

NGC 4649 (M 60) is a luminous, E1/E2 elliptical galaxy with boxy, cored stellar isophotes. Much is known about this well-observed galaxy because of its high luminosity and proximity (15.6 Mpc: Tonry et al. 2001). Unlike other luminous group-centered elliptical galaxies, NGC 4649 has an unusually large galactic rotation, increasing along the major axis to about 110 km s^{-1} at 3.8 kpc. Because of its large line of sight rotation, we shall generally assume for simplicity that NGC 4649 is viewed nearly perpendicular to its axis of rotation. Like many massive elliptical galaxies, NGC 4649 has a pair of low power radio jets each extending out 3 kpc from the galactic nucleus (Stanger & Warwick 1986; Shurkin et al. 2008).

The dashed line in Figure 1 shows the major axis rotation curve $v_{\text{rot}}(r)$ of NGC 4649 measured by De Bruyne et al. (2001) and Pinkney et al. (2003). The upper solid curve in Figure 1 shows the local circular velocity $v_{\text{circ}}(r)$ based on the combined mass of black hole, stars, and dark halo determined by Humphrey et al. (2008). Also plotted in Figure 1 as rising dotted lines are trajectories of gas that conserve the same specific angular momentum rv as that of the local stars at four observed radii. For example if all the hot gas at 3.8 kpc ($\log r = 0.6$) were rotating with the stars, as this gas flows inward it would spin up and collapse into a rotationally supported disk at $r_d \approx 1$ kpc where the rising dotted line intersects $v_{\text{circ}}(r)$. Such a large disk, which would be extremely obvious in the X-ray images of NGC 4649, has not formed (although smaller disks are possible). This rotational cooling flow catastrophe could be cited as an argument that the hot interstellar gas in elliptical galaxies cannot be flowing inward, but such a conclusion is unwarranted without further examination.

¹ We computed the X-ray ellipticity profile of NGC 4649 by applying the algorithm described in Buote et al. (2002) to the flat-fielded 0.3–7.0 keV image taken with the Chandra ACIS-S3 chip. To prevent X-ray point-sources from distorting the ellipticity profile, we first processed the image to remove all sources detected with the *wavdetect* tool (part of the CIAO 3.4 software package), following the procedure described in Fang, Humphrey & Buote (2009).

Figure 2 shows the apparent radial variation of the isophotal X-ray ellipticity $\epsilon_X(r)$ of NGC 4649 observed with Chandra by Diehl & Statler (2007) and more deeply by Humphrey¹. Some of the observational uncertainty within about 0.5 kpc of the galactic center may be due to difficulties in identifying and removing bright point sources and to the larger pixel size relative to the elliptical image near the galactic center. However, the two sets of X-ray observations in this small central region are consistent within observational uncertainties and those of Humphrey are in good agreement with optical ellipticities. Over the radial range $0.5 \lesssim r \lesssim 10$ kpc, ϵ_X increases monotonically with decreasing galactic (major axis) radius. We interpret this important feature of $\epsilon_X(r)$ in NGC 4649 as a (somewhat diluted) spin-up flattening expected from the naive inflow argument in Figure 1.

It is significant that the radial variation of ϵ_X in Figure 2 beyond about 1 kpc is opposite to that of the ellipticity of the stellar image ϵ_* based on *R*-band observations of Peletier et al. (1990). Indeed, in the small region $0.5 \lesssim r \lesssim 1$ kpc ($-0.3 \lesssim \text{Log } r \lesssim 0$) it is likely that ϵ_X is larger than ϵ_* , i.e. the hot gas is flatter than the local starlight, a feature seen in many massive elliptical galaxies (Diehl & Statler 2007). Such a trend arises naturally if the hot gas flows inward and is spun up to rotate faster than the local stars. In an oblate stellar ellipsoid having a highly concentrated de Vaucouleurs-type profile the gravitational potential is always more spherical than the local stellar density contours because the potential contributed by the dense central core acts much like a point mass. The starlight in NGC 4649 is flattened only slightly by galactic rotation, i.e. $v_{\text{circ}} \gg v_{\text{rot}}$ (Fig. 1).

To explore further this argument for inflowing gas we consider a variety of alternative possibilities. First consider non-radiating hot gas that does not flow inward. If NGC 4649 is assumed to have an axisymmetric oblate geometry, the X-ray ellipticity ϵ_X of non-rotating, non-radiating hot gas in hydrostatic equilibrium in its slightly flattened stellar distribution must be less than about half that of the local stars ϵ_* if the stellar density is constant with radius and indeed is typically very much less due to its strong central density concentration (cf. Figure 2-13. of Binney & Tremaine 1987). If slowly rotating but non-radiating hot gas in such a galaxy has a virial temperature and specific angular momentum similar to that of the stars, ϵ_X will increase above the non-rotating case but certainly cannot exceed ϵ_* – i.e. as a firm upper limit the gas cannot rotate faster than the stars from which it was ejected. Finally, if the hot virialized gas is allowed to radiate and flow inward, its rotation velocity and ϵ_X will increase even further until at a small enough radius ϵ_X may exceed ϵ_* . This is the type of inflow spin-up that we observe in NGC 4649 where $\epsilon_X \gtrsim \epsilon_*$ is seen in a limited region in Figure 2. In the presence of inflowing, low-angular momentum gas from the circumgalactic halo region, as we expect in NGC 4649, $\epsilon_X \gtrsim \epsilon_*$ is even more difficult to achieve without inflow spin-up. In §9 we review evidence for inflow spin-up in other nearby X-ray luminous elliptical galaxies.

The rotational cooling inflow catastrophe toward large disk formation in NGC 4649 (as in Fig. 1) can be mitigated by the influence of extended circumgalactic gas and interstellar turbulence. In view of its origin by cosmic ac-

cretion, the virialized hot gas in the extended group-scale gaseous halo around NGC 4649 probably has little or no global rotation. Consequently, the specific angular momentum of gas ejected from red giants rotating with the galaxy will be reduced as it mixes with gas of lower angular momentum flowing in from the halo. Mixing inflowing halo gas with stellar ejecta not only avoids forming large X-ray disks that are not observed, but also maintains the gas phase iron abundance close to that observed. In addition, it is well known that turbulent viscosity in the hot gas can spread angular momentum away from the axis of rotation, also reducing the likelihood of large disk formation. Turbulence can be driven by the intermittent release of AGN energy associated with a small accretion onto the central black hole as evidenced for example by the radio jets observed in NGC 4649. When circumgalactic inflow and turbulence are combined, it is possible to flatten the X-ray isophotes by an amount consistent with observation.

3. COMPUTATIONAL PROCEDURE

The gasdynamical equations that we use to describe rotating, non-turbulent gas flow in NGC 4649 are identical to those discussed in Brighenti & Mathews (2002) and Mathews & Brighenti (2003b):

$$\frac{\partial \rho}{\partial t} + \nabla \cdot \rho \mathbf{u} = \alpha \rho_* - q(T) \frac{\rho}{t_{\text{cool}}} \quad (1)$$

$$\rho \frac{d\mathbf{u}}{dt} = \rho \left[\frac{\partial \mathbf{u}}{\partial t} + (\mathbf{u} \cdot \nabla) \mathbf{u} \right] = -\nabla P - \rho \nabla \Phi - \alpha \rho_* (\mathbf{u} - \mathbf{u}_*), \quad (2)$$

and

$$\rho \frac{d\varepsilon}{dt} - \frac{P}{\rho} \frac{d\rho}{dt} = -\frac{\rho^2 \Lambda}{m_p^2} + \alpha \rho_* \left[\varepsilon_o - \frac{P}{\rho} - \varepsilon + \frac{1}{2} |\mathbf{u} - \mathbf{u}_*|^2 \right] \quad (3)$$

where $\varepsilon = 3kT/2\mu m_p$ is the specific thermal energy. The specific rate that mass is lost from an old stellar population of initial mass M_* is approximated with $\alpha_*(t) = 4.7 \times 10^{-20} (t/t_n)^{-1.3} \text{ s}^{-1}$ where $t_n = 13$ Gyrs (Mathews 1989). We assume that all of the gas ejected from evolving red giants eventually merges with the hot gas and C and N abundances in the hot gas provide evidence that this assumption is reasonable (Werner et al. 2006)². Gas at temperature T and abundance z loses thermal energy at a rate $-(\rho/m_p)^2 \Lambda(T, z) \text{ erg cm}^{-3} \text{ s}^{-1}$. We adopt the cooling coefficient of Sutherland and Dopita (1993), $n_{\text{ions}} n_e \Lambda_{sd}(T, z) \text{ erg cm}^{-3} \text{ s}^{-1}$, where in Equation 3 $\Lambda = [(4 - 3\mu)(2 + \mu)/25\mu^2] \Lambda_{sd}$ and $\mu = 0.61$ is the molecular weight.

² The assumption that a significant fraction of the mass lost from orbiting, mass-losing stars is eventually incorporated into the hot interstellar gas in elliptical galaxies has been considered for many years (e.g. Mathews 1990; Mathews & Brighenti 2003b). Parriott & Bregman (2008) and Bregman & Parriott (2009) provide recent, somewhat contrasting, computational studies of the interaction of gas ejected from mass-losing stars with ambient hot gas at rest. It is likely that some fraction of the stellar ejecta resides briefly in small clouds of warm $T \sim 10^4 \text{ K}$ gas ionized by the diffuse UV of old post-asymptotic branch stars. This gas is thought to be the source of diffuse optical line emission typically observed in elliptical galaxies. However, the lifetime of this warm gas cannot exceed about 10^6 yrs since otherwise its collective optical line luminosity would exceed values typically observed (Mathews 1990). Because of their large

As discussed above, gas cannot simply flow into the core of NGC 4649 and accumulate there over most of the Hubble time, because the total mass in and near the central black hole would be much larger than observed. Centrally inflowing gas must therefore flow out from the core in a manner consistent with the observed X-ray image, which, as we show here, resembles a cooling inflow. Since we do not treat the mass outflow in this paper, inflowing gas in our calculations does in fact cool in the central grid zone or onto a disk in the $z = 0$ plane. We consider two different ways of treating the inner boundary condition where gas cools: (1) allow cooled gas in central or disk zones to remain there at some low temperature (we choose $T = 10^4$ K) and be supported by internal pressure or rotation, or (2) remove cold gas from these zones as it begins to cool, allowing only hot gas to appear on the grid. To implement this second approach we include a mass sink term in the continuity equation $q(T)\rho/t_{cool}$ where $t_{cool} = 5m_p kT/2\mu\rho\Lambda$ is the local radiative cooling time at constant pressure. Furthermore, the dimensionless coefficient $q(T)$ is chosen to depend very sensitively on gas temperature so that gas is only removed when its temperature drops below about 10^6 K,

$$q(T) = q_{cool} \exp\left(-\frac{T}{T_{cool}}\right)^2 \quad (4)$$

where $q_{cool} = 2$ and $T_{cool} = 5 \times 10^5$ K. Except for the central zones, this gas removal scheme has no effect on the flow where $T \gg T_{cool}$. (Brighenti & Mathews 2002).

The source terms $\alpha_*\rho_*(\varepsilon_o - P/\rho - \varepsilon)$ in equation (3) represent the heating of the hot interstellar gas of specific energy ε by the mean energy of stellar ejecta ε_o less the work done P/ρ in displacing the hot gas. The mean gas injection energy is $\varepsilon_o = 3kT_o/2\mu m_p$ where $T_o = (\alpha_*T_* + \alpha_{sn}T_{sn})/(\alpha_* + \alpha_{sn})$. The stellar temperature T_* can be found by solving the Jeans equation, but this term is small and it is sufficient to use the approximation, $T_* = (\mu m_p/k)\sigma_*^2$, where σ_* is the local observed stellar velocity dispersion in the galaxy.

Heating by Type Ia supernovae, each of energy $E_{sn} \approx 10^{51}$ ergs, is assumed to be smoothly distributed in the hot gas and is described by multiplying the characteristic temperature of the mass M_{sn} ejected, $T_{sn} = 2\mu m_p E_{sn}/3kM_{sn}$, by the specific mass loss rate from supernovae, $\alpha_{sn} = 3.17 \times 10^{-20} \text{SNU}(t)(M_{sn}/M_\odot)\Upsilon_B^{-1} \text{s}^{-1}$, where $\Upsilon_B = 7.5$ is the assumed B -band stellar mass to light ratio. The supernova rate is expressed in traditional SNU-units, i.e. the number of supernovae in 100 yrs expected from stars of total luminosity $10^{10}L_{B\odot}$. In this paper we adopt a constant supernova rate $\text{SNU} = 0.06$ which is considerably lower than the approximate observed value for E + S0 galaxies $\text{SNU} = 0.16$ (Cappellaro et al. 1999). The Type Ia supernova rate of Cappellaro et al. is so high that many ellipticals that are known to contain hot virialized gas would rapidly develop winds and become essentially gas-free.

For the stellar mass profile in NGC 4649 we integrate a numerical fit to the J-band luminosity density given in Figure 2 of Humphrey et al. (2008) using a mass to light ratio $M_*/L_J = 1.43$ in solar units. The total stel-

lar mass is $2.32 \times 10^{11} M_\odot$. For simplicity we adopt a spherical E0 model for NGC 4649 which should be a good approximation even in the presence of the observed stellar rotation which is much less than the circular velocity (Fig. 1). Also recall that the gravitational potential of oblate ellipsoidal elliptical galaxies (with centrally peaked density profiles) is more spherical than the local equal-density contours. The dark NFW halo is described by a virial mass $M_v = 3.3 \times 10^{13} M_\odot$ with concentration $c = 13.5$ (Humphrey et al. 2006, 2008). Finally, the central black hole has mass $3.35 \times 10^9 M_\odot$. The stellar temperature distribution was found by assuming a virial relation $T_*(r) = (\mu m_p/k)\sigma_*(r)^2$ where the stellar velocity dispersion is a fit to the observations of Pinkney et al. (2003) ($r < 2.2$ kpc) and De Bruyne et al. (2001) ($r > 2.2$ kpc).

The major axis rotation velocity of NGC 4649 $v_{rot}(r)$ is also taken from the observations of De Bruyne et al. (2001) and Pinkney et al. (2003) along the major axis with $v_{rot}(r)$ assumed to be constant beyond the most distant observation. Since there is very little rotation along the minor axis, we assume a simple cosine variation to describe the two dimensional galactic rotation, $v_*(R, z) = v_{rot}(r)\cos(\theta)$ where $r = (R^2 + z^2)^{1/2}$, is the spherical radius, $\theta = \arctan(z/r)$ is the angle relative to the major axis plane and $v_{rot}(r)$ is the stellar rotation observed along the major axis.

Turbulent viscosity is essential to interpret the observed variation of X-ray isophotal ellipticity in NGC 4649. Since the rotational component of the gas velocity is typically much greater than that in the meridional plane, we consider only the viscous transport of the azimuthal gas velocity component v_ϕ . Our treatment of the viscous modification of the angular momentum density $\rho R v_\phi$ follows the same prescription as described in detail in Brighenti & Mathews (2000) to which the reader is referred. We also include a (small) viscous dissipation term in the thermal energy equation as described in Brighenti & Mathews (2000)³.

We assume that the turbulent viscosity can be expressed as a combination of dimensionally correct factors,

$$\mu(R, z) = \rho(R, z) \cdot v_t \cdot f r \quad (5)$$

where r is the radial coordinate, $\rho(R, z)$ is the computed gas density profile in cylindrical coordinates R, z , v_t is a characteristic turbulent velocity and $f r$ is the characteristic mean free path of the largest turbulent eddies where $f < 1$. Since these parameters appear only as a product, only one parameter $v_t f$ characterizes each solution. The objective is to find the minimum viscosity $\mu(r)$ consistent with the observed X-ray ellipticity (Fig. 2).

In principle the problem we address is somewhat ill-posed because of (1) unavoidable multi-Gyr transients

³ In this treatment we model the viscous terms directly as in the Navier-Stokes approximation (with additional energy dissipation) in which all terms are computed on the computational grid. We consider only the dominant viscosity contributed by the largest turbulent elements, approximated with a single parametrized viscosity. Recently Scannapieco & Brueggen (2008) have developed an alternative computational model for turbulence that includes dynamical contributions from subgrid levels, although in this treatment additional unspecified coefficients must be determined by comparing solutions with more detailed simulations or laboratory experiments.

surface to volume ratios, these small warm clouds probably merge into the hot interstellar gas by conductive heating.

and (2) the intrinsic time variability of important parameters. Regarding the first point, suppose (as we usually do) that the initial hot gas galactic atmosphere has the observed radial gas density and temperature profiles but is at rest with no rotation. As rotation is induced by stellar mass loss (from the term $\alpha\rho_*(\mathbf{u} - \mathbf{u}_*)$ in eq. 2) the interstellar gas spins up and an inward flow develops because of radiative losses. These transient adjustments can take many Gyrs. Consequently, we have decided to (rather arbitrarily) select 6 Gyrs as a time to view all models. As we describe below, a few flows have nearly reached a steady state by this time while others may still be slowly evolving. Secondly, the stellar mass loss rate and supernova rate are expected to change with time as the galactic stellar population evolves. However, to include this change introduces additional uncertainties and time dependences that we believe complicate our assessment of the gas flow velocity in present-day elliptical galaxies. For this reason we have decided to keep the stellar mass loss rate and Type Ia supernova rate fixed at their adopted current values for all flow solutions: $\alpha_* = 4.70 \times 10^{-20} \text{ s}^{-1}$ and $\text{SNu} = 0.06$.

We also monitor the approximate iron abundance in the gas as the calculation proceeds using an additional continuity equation for iron,

$$\frac{\partial(\rho z)}{\partial t} + \nabla \cdot (\rho z) \mathbf{u} = \alpha_* \rho_* z_* + \alpha_{sn} \rho_* \frac{y_z}{M_{sn}} \xi \quad (6)$$

where $\xi = \rho/\rho_H$ and z is the iron abundance relative to hydrogen, i.e. $z = \rho_{Fe}/\rho_H$. The local gas phase iron abundance z appears in the radiative cooling coefficient $\Lambda(T, z)$, but this has very little influence on the overall gas dynamics.

As mass is ejected from evolving stars, its iron abundance is assumed to contribute instantaneously to the local gas. For this purpose we adopt a simple stellar iron profile

$$z_*(r) = z_{*0} \left[1 + \left(\frac{r}{r_{*c}} \right)^2 \right]^{-0.15} \quad (7)$$

typical for large elliptical galaxies (e.g. Arimoto et al. 1997). In this last equation the stellar iron abundance is expressed in solar units, i.e. $z_{*0} = 1.82 \times 10^{-3}$. When circumgalactic gas is initially present, we assume that it has a uniform iron abundance $0.6z_{Fe,\odot}$ (see §7).

4. ONE-DIMENSIONAL COOLING FLOWS AND NUMERICAL STRATEGY FOR GAS REMOVAL

We begin with a discussion of simple one-dimensional, non-rotating solutions to the equations above in the presence of circumgalactic gas. The initial density profile for the circumgalactic gas is determined by integrating the equation of hydrostatic equilibrium toward larger radii, normalizing the central density to obtain good agreement with the density and temperature profiles observed by Humphrey et al. (2006; 2008) within 20 kpc and assuming isothermal gas ($T = 10^7 \text{ K}$) beyond this radius. These one-dimensional solutions are useful in selecting a preferred mass sink term $q(T)$ for numerically removing cooled gas.

We create computational grids of different resolutions by selecting the central grid zone size Δr and successively increasing the zone size by a factor $(1 + \varepsilon)$. Figure 3

shows the radial gas density and temperature profiles after computing for 6 Gyrs on a spherical 1D grid, using three grid resolutions $\Delta r = 15, 150$ and 600 pc with $\varepsilon = 0.0568, 0.03196$ and 0.01508 respectively, from left to right in Figure 3. Each solution is presented with two different numerical procedures to treat cooling gas: $q = 0$ for which the centrally cooled gas remains in the computational grid (light solid lines) or $q = q(T)$ as in equation (4) where cooled gas is continuously removed after each computational time step (heavy solid lines).

The left pair of panels in Figure 3 shows number density and temperature profiles computed with the highest spatial resolution. For these flow solutions the gas temperature has a small positive gradient throughout most of the central region. Positive dT/dr often occurs in classical cooling flows when circumgalactic gas is present because the virial temperature in the dark halo exceeds that of the stellar potential alone (Mathews & Brighenti 2003b). However, within about 100 pc of the galactic center the temperature increases due to compression as the gas approaches the central black hole, a feature which is absent if the black hole is removed (cf. heavy dotted profiles in Fig. 3). This central temperature rise – for inflowing gas – is an essential attribute of massive black holes (Brighenti & Mathews 1999) and was used by Humphrey et al. (2008) to verify the presence of the central black hole in NGC 4649. However, as gas flows even closer to the black hole, it ultimately cools by radiative losses in a very small region inside the central temperature peak. Clearly, some physical process (that we do not include here) must intervene in this small region to avoid an excessive concentration of cooled gas. In any case, the central temperature rise in $r \lesssim 100 \text{ pc}$ is responsible for the high gas temperatures observed by Humphrey et al. in their central aperture.

For $r \gtrsim 30 \text{ pc}$ the high resolution solutions with $\Delta r = 15 \text{ pc}$ are in good agreement with each other regardless of the numerical treatment of cooling gas, $q = 0$ or $q = q(T) \neq 0$. Note that the high resolution temperature profile in Figure 3 beyond about 1 kpc is slightly lower than the observed temperature at all radii. (The temperature profile computed in the two-dimensional version of this flow agrees better with the observations presumably because the flow velocity is less constrained in two dimensions.) These high-resolution one-dimensional flows are unable to reproduce the small observed negative gas temperature gradient observed in the region $0.2 \lesssim r \lesssim 1.5 \text{ kpc}$ ($-0.7 \lesssim \text{Log} r \lesssim 0.2$) which is largely unaffected by the potential of the central black hole. (This feature occurs naturally in two-dimensional flows.) The observed gas density is fit nicely beyond about 1 kpc in these flows, but continues to rise above the observed density inside this radius. This is a standard shortcoming of all simple one-dimensional cooling flows as discussed in detail by Mathews & Brighenti (2003b).

The central and right panels in Figure 3 show the results of identical one-dimensional calculations performed with coarser grid resolutions, $\Delta r = 150$ and 600 pc . The central temperature peak produced by the black hole potential is not resolved in either of these calculations, but the computed temperature profiles now depend on the choice of q . When $q = 0$ (light lines) the accumulated cold gas resides in a sphere of radius Δr which produces an unphysical negative temperature gradient in adjacent

central grid zones. This may be due to a small compression as the subsonic inflow flows toward the barrier presented by a sphere of dense cooled gas in the central zone. When $\Delta r = 150$ pc this feature is seen only near $r \approx 300$ pc, but when $\Delta r = 600$ pc the temperature gradient is negative out to about 3 kpc. However, when cooled gas is continuously removed with $q = q(T)$ (heavy lines), the computed (positive) temperature gradient is in essential agreement at all resolutions Δr . As a result of this numerical experiment, we shall remove cooling gas using the expression for $q(T)$ in equation (4) in all two-dimensional calculations where ΔR and Δz are typically much larger than 15 pc.

5. TWO-DIMENSIONAL FLOWS: INDIVIDUAL INFLUENCE OF CIRCUMGALACTIC GAS AND TURBULENCE

5.1. Without Circumgalactic Gas or Turbulence

To verify that a rotational cooling flow catastrophe could in fact occur in NGC 4649, we begin our two dimensional calculations with a non-turbulent flow in which galactic stars are the only source of hot gas, i.e. we do not include group-scale gas at any radius. The computed flow after 6 Gyrs is shown in the left panels of Figure 4. Since stellar mass loss and supernova rates are held constant, as discussed above, this solution reaches a steady state after only ~ 2 Gyrs and remains essentially unchanged afterwards. Gas ejected from stars is heated to the galactic virial temperature by gravitational compression and by the source terms in equation 3. The top left panel in Figure 4 shows that the computed (and azimuthally averaged) gas density (solid line) is much less than that observed by Humphrey et al. (filled circles) and this discrepancy increases with galactic radius beyond 10 kpc. This density shortfall arises because the stellar mass loss rate is unable to replenish gas at the same rate that it cools by radiative losses and flows into the cooling disk near the galactic core. The computed gas temperature is also much cooler than the observations because the local virial temperature associated with the stars $\sim T_*$ is less than that in the surrounding dark halo. The lower left panel in Figure 4 shows an image of the computed flow viewed in bolometric X-ray emission. The intense X-ray emission that results as gas cools toward the rotationally supported disk of radius ~ 1.8 kpc dominates the entire X-ray appearance of the galaxy. These computed X-ray isophotes have little resemblance to those observed in NGC 4649 (dashed lines) or observations of any other known elliptical galaxy. This verifies our prediction of a large X-ray disk for NGC 4649 in the absence of circumgalactic gas and turbulent viscosity.

5.2. With Turbulence but Without Circumgalactic Gas

The central panels in Figure 4 show flow profiles and isophotes computed for NGC 4649 after 6 Gyrs when gas viscosity is included but again without circumgalactic gas so stellar mass loss is the only source of gas. Turbulence in this flow is described with parameters $v_t = 50$ km s $^{-1}$ and $f = 0.1$ as defined in equation (5). The spatial variation of $\mu(R, z)$ can be seen in Figure 5 where we plot $\mu(R, 0)$ and $\mu(0, z)$ for $v_t = 50$ km s $^{-1}$ and $f = 0.05$ (parameters appropriate for the “reference model” discussed below). The density profile in this solution is improved but is still too low overall because of the inability of old galactic stars to resupply gas as it flows

inward by radiative losses. The temperature profile is marginally improved but is still much lower than observed by Humphrey et al. (2008). However, the X-ray isophotes for this model are greatly improved and are in good agreement with observation, considering the uncertainties in the observed ellipticity $\epsilon_X(r)$ shown in Figure 2. Because of observational uncertainties in $\epsilon_X(r)$ within about 0.5 kpc, it is not possible to compare computed and observed isophotes in this central region. But it is clear that subsonic turbulence must be an essential component in successful flow models for NGC 4649.

5.3. With Circumgalactic Gas but Without Turbulence

The gas density in NGC 4649 is not expected to drop to zero just beyond 20 kpc, the most distant density observation by Humphrey et al. (2008). In all subsequent computed gas flows discussed here we adopt an initially stationary gas density profile that matches the observations of NGC 4649 out to 20 kpc but is extrapolated further by solving the equation of hydrostatic equilibrium for an isothermal gas ($T = 10^7$ K) at rest in the potential of the stellar and dark halo mass described above. The initial density profile extrapolated in this manner beyond 20 kpc has the same logarithmic slope as the observations between 1 and 20 kpc. While the gas density is low in this extrapolated region, the total mass of this gas exceeds that observed within 20 kpc.

The gas flow computed with circumgalactic gas but without viscosity is shown in the panels on the right in Figure 4. The gas density and temperature profiles are now in much better agreement with observations than previous flows without circumgalactic gas. After 6 Gyrs the inflowing circumgalactic gas continues to create density and temperature profiles that agree with observations of NGC 4649 within 20 kpc. Indeed, this agreement is another indirect argument for cooling inflow. (The temperature downturn in the central grid zone is an artifact of incomplete removal of cooling gas at this moment in the calculation.) Beyond about 1.5 kpc, the computed X-ray isophotes are in reasonably good agreement with observations. However, in the range $0.5 \lesssim r \lesssim 1.5$ kpc the computed X-ray isophotes are still much flatter than those observed in NGC 4649. We conclude that circumgalactic gas improves the agreement with observations but cannot by itself provide completely satisfactory flow solutions.

The reduced prominence of the X-ray disk when circumgalactic gas is included occurs because we assume that the initial circumgalactic gas is not rotating. Non-rotating gas flowing toward NGC 4649 from the group-scale halo provides an inertial brake on gas ejected from evolving stars that systematically share the galactic rotation. But spin-up and disk formation still occur at a level that is inconsistent with observation (lower right panel in Fig. 4). If we had allowed for the time-dependent decrease in the stellar mass loss rate expected as a single stellar population evolves, $\dot{M}_* \propto t^{-1.3}$, the size of the cooling disk would be even larger than shown at the bottom right in Figure 4 because of the increased mass of high-angular momentum gas introduced in the past. In this sense our central disk sizes computed with constant α_* are conservative.

Because of inadequacies in the solutions shown in Fig-

ure 4, we now explore whether the formation of large, X-ray detectable disks can be avoided by considering both the turbulent redistribution of angular momentum and rotational suppression by mixing with non-rotating circumgalactic gas.

6. 2D FLOWS WITH BOTH TURBULENCE AND CIRCUMGALACTIC GAS

We now describe three representative evolutionary gas flows in which the initial density and temperature profiles are extrapolated into the circumgalactic halo beyond the observations as described above. All gas is assumed to be initially at rest, but it acquires a small radial inflow due to radiative losses and angular momentum is supplied by mass ejected from evolving stars in the rotating galaxy.

6.1. Reference Model

The left panels in Figure 6 show gas density and temperature profiles and X-ray isophotes for NGC 4649 computed after 6 Gyrs with viscosity parameters $v_t = 50 \text{ km s}^{-1}$ and $f = 0.05$ for this “reference model”. At this time the computed temperature and density are in good agreement with observed profiles. The central temperature peak due to the black hole is not resolved at the grid resolution used, (central $\Delta R = \Delta z = 150 \text{ pc}$). Furthermore, at this resolution the flow near the very center is artificially disturbed when gas cools rapidly in the central zones. In the left panels we show typical flow excursions at three times. The X-ray isophotes beyond $\sim 0.5 \text{ kpc}$ also follow the observed $\epsilon_X(r)$ within acceptable uncertainties. Because of possible uncertainties in $\epsilon_X(r)$ within 0.5 kpc – both observational (Fig. 2) and computational – it is not possible to make a detailed comparison of our flow with observations in this important region. However, the central rotation has not completely disappeared in this flow and gas continues to cool into a small disk of radius $\sim 300 \text{ pc}$. It is significant that this disk is similar in size to the small dusty disks discovered with the Hubble Space Telescope in the cores of many elliptical galaxies (e.g. Lauer et al. 2005). With deeper Chandra observations the gas flowing into these small disks may become visible in X-ray images.

Rotation is helpful in achieving a better agreement with azimuthally averaged gas density and temperature profiles in the left panels of Figure 6. The rotational flattening visible in the computed X-ray isophotes near the core of this flow (lower left panel) causes the azimuthally averaged gas density to flatten similar to the observations of NGC 4649. In addition, rotation introduces a shallow negative temperature gradient in the range $0.2 \lesssim r \lesssim 1 \text{ kpc}$ ($-0.7 \lesssim \text{Log} r \lesssim 0$) that is unrelated to the black hole potential. This arises because of compressional heating as gas flows toward the disk. Neither the central density flattening or the shallow negative dT/dr within $\sim 1 \text{ kpc}$ appear in otherwise similar 1D spherical flows.

The turbulent velocity $v_t = 50 \text{ km s}^{-1}$ in this flow is much less than the sound speed in the hot gas in NGC 4649 beyond about 1 kpc , $c_s \approx 460 \text{ km s}^{-1}$. As a result, the ratio of turbulent to gas pressure $P_t/P = (v_t/c_s)^2 \approx 0.012$ is very small, provided the viscosity scale factor f exceeds $(v_t f)/c_s \approx 0.005$, which we think is likely. For a Kolmogorov spectrum the velocity of turbulent elements v varies with their size ℓ as $v \propto \ell^{1/3}$ so $\mu(\ell) \propto v\ell \propto \ell^{4/3}$ and most of the momentum is carried by the larger ed-

dies; this argues against adopting very small values of $f \sim \ell/r$ and ℓ for a fixed turbulent velocity at any radius r . Determinations of the underlying mass by Humphrey et al. (2008) using hydrostatic equilibrium implicitly require $P_t/P \ll 1$ which is consistent with the level of turbulence required to remove unobserved large X-ray disks in NGC 4649. Finally we note that the agreement with observed X-ray isophotal ellipticity could be improved with a more highly parameterized and finely-tuned function for $\mu(R, z)$, but we do not pursue this alternative here. Altogether, we regard this as a successful model and refer to it subsequently as the “reference model”.

While the agreement between our 2D reference model and X-ray observations of NGC 4649 is quite satisfactory, it is useful to keep in mind some of the approximations we have made: NGC 4649 is assumed to be viewed perpendicular to its rotation, we use a cosine law for $v(R, z)$ to interpolate between observations on the major and minor axes, we assume that the rates of stellar mass loss and supernova explosions are constant during the calculation, we compare with observations only after 6 Gyrs, our removal of cooled gas introduces intermittency in the central zones, our turbulent viscosity $\mu(R, z)$ is parameterized in a simple way, and viscosity is applied only to the azimuthal shear velocity. Consequently, exact agreements with the observations are not expected.

6.2. Additional Models

One of our objectives is to estimate the minimum turbulent viscosity and pressure necessary to bring the X-ray isophotes into agreement with X-ray observations of NGC 4649. Models with $v_t f$ less than that of the reference model tend to resemble the inadequate flow for NGC 4649 without turbulence (but including circumgalactic gas) shown in Figure 4. For example, the central panels of Figure 6 show the flow after 6 Gyrs computed with $v_t = 25 \text{ km s}^{-1}$ and $f = 0.025$. The gas density and temperature profiles in this flow are similar to the reference model, including excursions due to sudden cooling. However, the computed X-ray isophotes are unacceptably flat near $r \sim 1 \text{ kpc}$. Our overall subjective assessment of this model is that it is less successful than the reference model which can be regarded as an acceptable model having the smallest turbulent viscosity.

Finally, in the right panels of Figure 6 we explore the effect of a turbulent viscosity that exceeds that of the reference model, i.e. $v_t = 50 \text{ km s}^{-1}$ and $f = 0.1$. The X-ray isophotes are seen to be considerably rounder for this flow and are a reasonable match to the observations beyond about 0.5 kpc from the center. However, for this solution the flow approaches that of a non-rotating pure cooling flow with density that is too high (for $r \lesssim 0.7 \text{ kpc}$) and with a temperature gradient that remains positive in the range $0.2 \lesssim r \lesssim 1 \text{ kpc}$. Consequently, we regard this model as less successful overall than the reference model for NGC 4649.

7. APPROXIMATE GAS ABUNDANCE PROFILES

The gas phase iron abundance profile in NGC 4649 depends on the Type Ia supernova rate ($\text{SNU} = 0.06$), the stellar abundance profile $z_*(r)$ (given by equation 7 with parameters $z_{*0} = 1.5z_\odot$ with solar abundance $z_\odot = 1.82 \times 10^{-3}$, $r_{*c} = 100 \text{ pc}$), the assumed (constant) iron abundance in the circumgalactic gas $z_{cgg} = 0.6z_\odot$,

and the time elapsed since the beginning of the calculation. Figure 7 shows hot gas iron abundance profiles computed to 6 Gyrs for two flows discussed above. The heavy solid line shows z_{Fe}/z_{\odot} with inflowing circumgalactic gas and with reference model viscosity parameters ($v_t = 50 \text{ km s}^{-1}$ and $f = 0.05$). In general the abundance profile tends to flatten slightly with increasing turbulent viscosity, but we do not illustrate these details. This abundance profile agrees rather closely with the abundance data in Figure 7 based on observations described in Humphrey et al. (2007).

The thin line in Figure 7 shows the abundance profiles for the same flow parameters but without circumgalactic gas. In flows without circumgalactic gas after 6 Gyrs the gas abundance approaches ~ 3.6 times solar with or without turbulent viscosity. Since gas-phase iron abundances this high are rarely if ever observed, Figure 7 provides dramatic evidence that low-abundance circumgalactic gas must flow slowly in from the extended halo, as in a normal cooling flow, diluting the enrichment received from galactic supernovae.

8. HIGHER COMPUTATIONAL RESOLUTION

In Figure 8 we show a high resolution 2D 6-Gyr calculation of the reference flow in which the grid is uniform for $R, z < 5 \text{ kpc}$, with $\Delta R = \Delta z = 33 \text{ pc}$ (i.e. ~ 150 uniform zones in R and z). Then the grid extends for another 150 zones in both directions with increasing zone size to reach the outer boundary at 190 kpc. At this higher resolution the gas density and temperature profiles follow the observations within 1 kpc even more closely than with normal resolution (left panels in Figure 6). However, the central temperature peak is not as sharp as in the 1D high resolution flow in Figure 3. This is probably due to unrealistically large (subsonic) meridional velocities in the R, z -plane near the center – our current viscosity prescription only damps the azimuthal component of the gas velocity. The bolometric X-ray image is essentially indistinguishable from the reference flow in Figure 6. It is important to note that our flows at high resolution do not oscillate unrealistically near the center as mass is removed by cooling. This is probably due to the smaller mass that is removed from smaller central zones that causes relatively less disturbance in nearby zones.

The top panels in Figure 8 show the influence of viscosity on the density and temperature profiles. As the viscosity increases, the temperature profile becomes flatter and the density profile steepens. This sensitivity of the central temperature profile in $-0.5 \lesssim \text{Logr} \lesssim 0$ ($0.3 \lesssim r \lesssim 1 \text{ kpc}$) is a measure of the role of viscosity in rotating, quasi-disk like flows in this region. This is an interesting detail that should be explored in other X-ray luminous elliptical galaxies. As before, identical flows without a central black hole show no central temperature peak inside 300 pc.

The bottom panels in Figure 8 shows the X-ray isophotes and the gas velocity field in the high-resolution reference flow superimposed on the local X-ray isophotes. The snake-like flow in the central few kpc is characteristic of all our solutions and also occurs in flows that are not rotating. We believe that this non-radial flow pattern may result as the inflow adjusts to accommodate gas recently ejected from stars that enters the flow with

a radial gradient that is steeper than the local gas density profile in hydrostatic equilibrium. These velocities have spatial scales that are similar to those observed in optical emission lines in luminous elliptical galaxies (Caon, Machetto & Pastoriza 2000), but the observed velocities are somewhat higher. The velocity field varies with time, causing the X-ray profiles to distort and wander slightly from those at 6 Gyrs shown in Figure 8. The X-ray ellipticity can be estimated with $\epsilon_X = 1 - z_i/R_i$ where z_i and R_i are the intercepts of X-ray isophotes on the z and R axes in Figure 8. These approximate ellipticities, shown as crosses in Figure 2, are in good agreement with observed values. While X-ray observations in Figure 2 indicate that $\epsilon_X > \epsilon_*$ near 0.6 kpc ($\log r = -0.2$), the observations of Humphrey (open circles) suggest that $\epsilon_X \approx \epsilon_*$ closer to the origin. This near equality could arise if viscous damping increases more strongly toward the center than in our computed flows, allowing a nearly spherical flow of gas onto the central black hole in NGC 4649. The crosses in Figure 1 show the tangential gas velocity along the major (z) axis for the high resolution flow in Figure 8. Because of inflow spin-up, the gas rotates faster than the stars for $r \lesssim 2 \text{ kpc}$.

9. CHANDRA EVIDENCE OF ROTATIONAL INFLOW IN OTHER ELLIPTICAL GALAXIES

In their recent analysis of Chandra X-ray images observed in 54 elliptical galaxies Diehl & Statler (2007) found no convincing correlations between the X-ray appearance and the rotation of the galactic stars or the shape of the stellar potential. Specifically, they found no clear relationship between the mean X-ray ellipticity and line of sight stellar rotational velocity, both averaged over $0.6 - 0.9R_J$ where R_J is the J-band effective radius of the galactic stars. Furthermore, their plots of the X-ray ellipticity $\langle \epsilon_X(0.6 - 0.9R_J) \rangle$ against either the stellar ellipticity $\langle \epsilon_*(0.6 - 0.9R_J) \rangle$ or the stellar rotation $\langle v_{rot}(0.6 - 0.9R_J) \rangle$ show large scatter without an obvious correlation. (They do not consider the effective potential of the X-ray gas in its locally rotating frame.) These results led Diehl & Statler to conclude that the hot gas in elliptical galaxies is quite far from hydrostatic equilibrium and that rotation cannot be the dominant factor that produces the hot gas X-ray ellipticities they observe.

However, we suspect that conclusions based on X-ray ellipticities and stellar properties, when spatially averaged over the broad radial range $0.6 - 0.9R_J$, may be insensitive to regular trends in the X-ray and stellar ellipticity profiles apparent in the unaveraged, raw data (Fig. 5 of Diehl & Statler 2007). For example, for NGC 4649 Diehl & Statler find that the X-ray ellipticity $\langle \epsilon_X(0.6 - 0.9R_J) \rangle = 0.08 \pm 0.03$ is less than the corresponding stellar ellipticity $\langle \epsilon_*(0.6 - 0.9R_J) \rangle = 0.18 \pm 0.01$, and, for similar galaxies in their complete sample, Diehl & Statler infer that the hot gas is not rotating or is insensitive to the flattened stellar potential in this annular bin. However, we interpret the negative slope $d\epsilon_X/dr$ in NGC 4649 (Fig. 2) beyond about 0.5 kpc ($0.14R_J$) as clear evidence of rotational spin-up resulting from a global inflow of the X-ray emitting gas. Rotational spin-up of the hot interstellar gas cannot be accurately inferred from absolute values of ellipticity or the line of sight velocity at any particular radius. Instead, in the mitigating presence of turbulence and/or circumgalactic gas, rotational spin-up

can only be detected by the radial trend of X-ray isophotal flattening, $d\epsilon_X/dr < 0$, particularly when $\epsilon_X > \epsilon_*$ near the center of the galaxy, implying that the gas is rotating faster than the local stars.

To explore our interpretation further, we examine the detailed Chandra data of $\epsilon_X(r)$ and $\epsilon_*(r)$ for 36 well-observed galaxies in Figure 5 of Diehl & Statler (2007). We do not consider six of these galaxies (NGC 193, 383, 507, 1316, 1553, and 4526) since their morphological classification parameter T from LEDA exceeds -4.0, suggesting that they are E/S0 or later, although our conclusions are independent of this sample refinement. With this reduced sample of 30 E galaxies, we subjectively classified the innermost slope $d\epsilon_X/dr$ into positive (+), indeterminate (0) and negative (-). We find the number of galaxies in each slope category to be (+,0,-) = (4,10,16), showing that a majority of Chandra-observed E galaxies have negative $d\epsilon_X/dr$ as expected from inflow spin-up⁴.

However, some of these galaxies have been observed at only 1 - 3 radii within R_J either because of their large distance and reduced spatial scale or because of the relatively low total number of Chandra photons available. To allow for this, we consider a smaller subsample of 16 E galaxies, including NGC 4649, in which ϵ_X has been measured at four or more radii $\leq R_J$. For this well-observed subsample we find overwhelming evidence for rotational spin-up in $r \lesssim R_J$: (+,0,-) = (2,2,12). Those few galaxies with indeterminate or positive $d\epsilon_X/dr$ may have spin axes that are closer to our line of sight or their ordered rotation may have been masked by transient kinematical activity following a recent AGN outburst – such asymmetric AGN disturbances in elliptical galaxies have been studied and quantified in detail by Diehl & Statler (2008a).

In addition, for the 12 E galaxies showing clear evidence of inflow spin-up, $d\epsilon_X/dr < 0$, the stellar and X-ray (major axis) position angles are in good agreement either near the galaxy center or closer to R_J where most of the stellar mass loss and angular momentum may be deposited. Finally, of the 12 galaxies with strong evidence of inflowing rotational spin-up ($d\epsilon_X/dr < 0$), the innermost measured X-ray ellipticity in 10 galaxies exceeds the ellipticity of local stars. Since the stellar gravitational potential in giant elliptical galaxies is always more spherical than the local ellipsoidal stellar density distribution, this ellipticity excess cannot be understood as non-rotating gas nearly in hydrostatic equilibrium in the flattened stellar potential or gas rotating with the local stars. Instead, $\epsilon_X > \epsilon_*$ indicates that the inner hot gas in these 12 galaxies is rotating faster than the local stars, as a natural consequence of inflowing spin-up.

Nevertheless, the absence of any clear correlations among broadly binned averages, $\langle \epsilon_X(0.6 - 0.9R_J) \rangle$ and $\langle \epsilon_*(0.6 - 0.9R_J) \rangle$ or $\langle \epsilon_X(0.6 - 0.9R_J) \rangle$ and $\langle v_{rot}(0.6 - 0.9R_J) \rangle$, as found by Diehl & Statler (2007) in their complete sample, is interesting and should be better understood. We believe that several factors combine to explain the scatter in these plots. The mass of inflowing circumgalactic, group-scale gas increases with the mass of the

surrounding dark halo which is highly variable among optically similar elliptical galaxies (Mathews et al. 2006b). As a result, the fractional contribution of inflowing (non-rotating) circumgalactic gas in the hot gas near the galactic effective radius is expected to vary considerably. For a given rotation of the stellar system, the X-ray ellipticity should decrease inversely with the local fraction of circumgalactic gas. This introduces a stochastic variation in $\langle \epsilon_X(0.6 - 0.9R_J) \rangle$ that is unrelated to inflow spin-up. Secondly, we have shown here that the X-ray ellipticity and its radial variation depends somewhat on large scale subsonic velocity fields in the hot gas. These velocities are weakly time-dependent and may depend on the radial distribution (and age) of mass-losing stars which may vary among the galaxies in the sample considered by Diehl & Statler. Finally, the unknown turbulent viscosity profile in the hot gas may alter $\epsilon_X(r)$ in complicated and unpredictable ways because of occasional energy outbursts associated with AGN feedback from the central black hole. During the period of transient recovery following each AGN outburst, the systematic spatial and kinematic patterns in the hot gas are likely to be significantly disturbed.

10. SUMMARY OF OBSERVATIONAL EVIDENCE FOR COOLING INFLOW

Throughout the preceding discussion we mentioned several arguments why the X-ray emitting gas in NGC 4649 – and in other massive elliptical galaxies – appears to be undergoing inflow. In view of the remarkable implications of these observational and theoretical arguments, it is useful to summarize them again here.

(1) *Increasing ellipticity of X-ray isophotes toward the galactic center, often exceeding that of local stars:* We have shown that this can arise naturally from angular momentum spin-up of inflowing gas driven by mass ejected from stars that collectively follow the global galactic rotation. In many large elliptical galaxies the central X-ray ellipticity exceeds that of the stars, indicating that the hot gas cannot be rotating with the stars in their potential, but must have a faster rotation due to inflow spin-up.

(2) *Central peak in gas temperature due to compression as gas flows in toward a centrally concentrated potential:* Temperature peaks occur as inflowing gas approaches a massive black hole (Fig. 3) or flows onto a small central disk orbiting the black hole (e.g. the reference model in the left panels of Figure 6). This temperature increase is a consequence of adiabatic heating as gas approaching the central black hole is compressed by the steepening potential.

(3) *Dusty, rotationally supported nuclear disks:* Dusty disks are observed in the cores of 40 - 50% of luminous elliptical galaxies (e.g. van Dokkum & Franx 1995; Lauer et al. 2005). Disks of this type are expected to form naturally from dust ejected by mass-losing red giant stars within ~ 1 kpc from the galactic center (Mathews & Brighenti 2003a). The absence of disks in other similar ellipticals suggests that AGN energy has disrupted them on time scales of $10^7 - 10^8$ yrs, consistent with the spatially extended dust observed by Temi, Brighenti & Mathews (2007). Indeed, highly transient, chaotically

⁴ Galaxies with -: IC 1262, 1459, NGC 720, 1399, 1404, 1407, 4125, 4261, 4374, 4406, 4552, 4636, 4649, 4697, 5846, 6482; with 0: IC 4296, NGC 741, 1132, 1549, 1600, 3923, 4472, 5018, 7052, 7618; with +: NGC 315, 533, 1700, 5044.

arranged dust clouds are observed in the cores of many ellipticals that do not contain disks.

(4) *Gas metal abundance*: Even though the hot gas inside elliptical galaxies is continuously enriched by Type Ia supernovae and mass-losing stars, the metal abundance observed in the hot gas is rarely much greater than that of the local stars. This can be understood by two aspects of inflow: (i) dilution of the hot gas metallicity by low metallicity gas flowing in from circumgalactic, group-scale halos and (ii) continuous removal of metal-rich gas on galactic scales. This latter removal could be simply a continuation of the circumgalactic cooling inflow but ultimately this metal-rich gas must cool or be transported far out into the hot gas in jets or buoyant regions. In principle, the iron from Type Ia supernovae may cool by radiative losses before it thermally merges with the hot gas; the main difficulty with this is the uncertain thermal conductivity imposed by the unknown local magnetic field topology (Brighenti & Mathews 2005).

(5) *Gas density and inflowing circumgalactic gas*: For galaxies like NGC 4649 the expected stellar mass loss rate from an old stellar population is insufficient to maintain the relatively high gas densities observed in the presence of inflow (e.g. Fig. 4). Without circumgalactic gas, the computed gas density becomes increasingly lower than the observed density at larger galactic radius. In addition, gas lost from red giant stars virializes to temperatures that are lower than those observed in NGC 4649, as seen beyond about 2 kpc in the left and central panels of Figure 4. However, both of these difficulties can be corrected by including a cooling inflow from circumgalactic gas virialized in the dark matter halos surrounding elliptical galaxies.

(6) *Similarity of observations and computed cooling flows*: The hot gas density and temperature profiles observed in massive ellipticals as well as the hot gas isophotes can be explained with gasdynamical models of inflowing, radiatively cooling gas (Figs. 6 & 8). The failure to observe cooling gas at intermediate temperatures can be understood by rapid dust-assisted cooling (Mathews & Brighenti 2003a), provided the cooling rate does not greatly exceed $\sim 1 M_{\odot} \text{ yr}^{-1}$. However, the time-integrated mass of cooled gas expected in elliptical galaxy cores is not observed, so the mass inflows we compute here cannot be sustained throughout the evolution of NGC 4649 or other massive ellipticals. Our cooling inflow model is a valid description of the *instantaneous* flow currently observed in NGC 4649. To be valid over cosmic times, it is necessary to consider the release of AGN accretion energy in the galactic core and associated outflows of energy and mass.

11. MASS ACCRETION RATE – FATE OF INFLOWING GAS

Figure 9 shows the rate $\dot{M}_{cool}(t)$ that gas cools in several flow models discussed here. In the absence of circumgalactic gas, the galactic cooling rate becomes nearly equal to the total galactic stellar mass loss rate, $\dot{M}_{cool} \approx 0.3 M_{\odot} \text{ yr}^{-1}$ following an initial transient adjustment. The computed cooling rate is essentially independent of the turbulent viscosity. When circumgalactic gas is included, $\dot{M}_{cool}(t)$ is somewhat larger $\sim 0.9 M_{\odot}$

yr^{-1} . This cooling rate is inconsistent with the much lower value $\dot{M}_{cool} \approx 0.05 M_{\odot} \text{ yr}^{-1}$ allowed by X-ray spectra and FUSE observations of the OVI 1032-1038 Å doublet in NGC 4649 (Bregman & Athey 2003).

This failure to observe cooling and cooled gas is the cooling flow problem. While the X-ray properties of NGC 4649 resemble a typical (weakly-rotating) cooling flow down to $r \sim 150$ pc, the innermost radius observed by Humphrey et al., there is no spectral evidence for cooling and no young stars are detected. The ultra-short (gas) radiative cooling time (6 Myr) and the (non-rotating) gas flow time to the center (0.5 Myr) at radius $r = 150$ pc concentrate and enhance the AGN feedback-cooling flow problem in NGC 4649 unlike that of any other known galaxy, group or cluster.

The currently preferred paradigm for solving the cooling flow problem, as explained in detail in the recent review by McNamara & Nulsen (2007), is that the hot gas is being heated by the creation of X-ray cavities or by the dissipation of outwardly propagating shock waves. According to this hypothesis, as the hot gas is heated in this manner, it experiences little or no systematic flow in either radial direction. But neither of these heating mechanisms seems likely in NGC 4649. Moreover, X-ray cavities formed with cosmic rays result not in heating but in global cooling due to an expansion of the entire gaseous atmosphere (Mathews & Brighenti 2008). Of course, cavities formed with ultra-hot (but non-relativistic) gas can increase the global thermal energy of the hot gas if the cavity gas mixes with the ambient, pre-cavity gas. In any case, no cavities larger than about 125 pc in radius are currently observed in NGC 4649 (Humphrey et al. 2008). Heating by wave dissipation occurs mostly in the central regions where the hot gas density gradient is flatter. Because of this, as wave heating continues for several Gyrs. the central gas becomes much hotter than that observed (Mathews, Faltenbacher & Brighenti 2006a).

Nevertheless, if the hot gas in NGC 4649 is being heated somehow by AGN energy so there is no cooling inflow, this heating must be nearly continuous in time and exquisitely fine-tuned with galactic radius to maintain the appearance of a normal cooling inflow complete with a central, constant-entropy temperature peak near the massive nuclear black hole in which the gas has a cooling time of only a few million years. However, the effect of inflow spin-up on the X-ray isophotes observed in NGC 4649 and other similar galaxies is clearly inconsistent with non-cooling flow models that stop the inflow with heating at every radius. Finally, we note again that the hot gas observed within the central elliptical galaxy must move radially to avoid extremely large iron abundances, assuming that Type Ia iron thermally merges into the hot gas – this is another difficult constraint when the cooling flow problem is solved with simple heating scenarios in which there is no radial flow of gas.

Most of the gas that cools in our computed flows (with circumgalactic gas) cannot have simply contributed to the mass of the central black hole in NGC 4649 since its mass would be reached after only ~ 3 Gyrs. It is also unclear how much cooling is occurring since rapid dust-assisted cooling (Mathews & Brighenti 2003a) would make cooling in elliptical galaxies difficult to detect in X-ray spectra. Certainly, the low apparent cooling rate

in NGC 4649 estimated from UV line emission, $\sim 0.05 M_{\odot} \text{ yr}^{-1}$, cannot be reconciled with the larger mass inflow rates in the models we compute here.

Since the X-ray evidence for global inflow is so compelling in NGC 4649, the most likely fate of the inflowing gas is that gas is being transported outward in a manner that is intermittent or not easily visible in X-ray images and spectra (Mathews, Brighenti & Buote 2004). Outward mass transport may occur either in jets (Brighenti & Mathews 2006) or in low density, buoyant outflows created for example with cosmic rays (Mathews & Brighenti 2008). Like many massive elliptical galaxies, NGC 4649 has a pair of low luminosity FRI radio jets. These jets may transport thermal gas from deep within the core of NGC 4649, provided they are similar to the mass-carrying radio jets found in Seyfert galaxies by Whittle & Wilson (2004). Some of the cooled gas and dust may also be intermittently removed from deep within NGC 4649 by jets or buoyant outflows as implied by far-IR dust emission observed out to 5-10 kpc in many elliptical galaxies (Temi, Brighenti & Mathews 2007). It is likely that the mass outflow in NGC 4649 is episodic and that we are viewing NGC 4649 at a quiescent moment between radio lobe outflow events when gas is undergoing a cooling inflow toward the center (e.g. Diehl & Statler 2008b).

12. CONCLUSIONS

We have shown that the X-ray emitting gas associated with the bright elliptical galaxy NGC 4649 has density and temperature profiles that can be understood as a rotating, radiatively cooling inflow with a mild turbulent viscosity. Evidence of inflow is present at every radius in NGC 4649. On the largest scales, a radiatively cooling inflow of circumgalactic gas is required to dilute the hot gas iron abundance acquired from supernovae down to observed values, assuming that the iron ejected by Type Ia supernovae does not cool by radiative losses before it merges with the ambient hot gas. The relatively high gas density and temperature observed in NGC 4649 beyond ~ 10 kpc can also be explained with inflowing circumgalactic gas. On intermediate galactic scales, observations of the X-ray ellipticity in NGC 4649 and other bright elliptical galaxies show that the hot gas is spun up by mass ejected from evolving stars that rotate collectively with the galaxy. Inflow spin-up is seen in the increasing X-ray isophotal ellipticity with decreasing galactic radius until it exceeds the ellipticity of the local stars near the galactic center. However, for NGC 4649, which rotates unusually fast for a massive boxy elliptical, a small turbulent viscosity is required to avoid forming multi-kpc X-ray disks that are not observed. The shallow negative temperature gradient inside ~ 1 kpc in NGC 4649 is X-ray evidence of an inflow that compresses toward a sub-kpc disk. The observed X-ray isophotes can be matched with a turbulent viscosity for which the corresponding turbulent pressure is much less than the gas pressure, so the integrated mass profiles found by assuming hydrostatic equilibrium (Humphrey et al. 2008) are unaffected. This alleviates the concern expressed by Diehl & Statler (2007) that the hot gas in elliptical galaxies is very far from hydrostatic equilibrium. Galactic

mass determinations based on X-ray thermal emission may fail for some elliptical galaxies where non-thermal pressure dominates the galactic core, such as NGC 4636 (Brighenti & Mathews 1997; Baldi et al. 2009), but this problem does not seem to occur in NGC 4649. On the smallest scales observed with Chandra, within about 100 parsecs, the central temperature peak in NGC 4649 discovered by Humphrey et al. (2008) is a natural consequence of subsonic cooling inflow. In spite of ongoing radiative losses, the central gas temperature increases due to (nearly adiabatic) compression as gas approaches the central black hole or the small disk around it. The kpc-scale negative temperature gradient in NGC 4649 formed as gas compresses toward a small disk is not caused by recent AGN heating since the gas entropy in this region increases with galactic radius. This type of central inflow is also consistent with nuclear disks of cooled dusty gas having radii of a few hundred parsecs commonly observed in the cores of luminous elliptical galaxies.

NGC 4649 represents the most concentrated known example of the cooling flow problem. The observed density and temperature profiles can be explained at every radius with a radiatively cooling inflow. At the smallest observable radius in NGC 4649, about 150 pc, the times for cooling and flow to the core are only a few million years. For this reason it will be very difficult to devise heating scenarios that maintain the gas at rest, perfectly mimicking a cooling inflow. No ideally heated model in which the hot gas in NGC 4649 remains stationary can account for commonly observed X-ray ellipticity profiles $\epsilon_X(r)$ that require inflow spin-up.

The current mass inflow rate in our successful calculations is $\sim 1 M_{\odot} \text{ yr}^{-1}$, but the stellar mass loss rate was certainly several times larger in the past. Consequently, if this flow continued over a Hubble time, the total mass of cooled gas accumulated in the galactic core of NGC 4649 would exceed the mass of the black hole and stars within ~ 1 kpc by factors of 3 - 10. Therefore, the mass inflow indicated by the central temperature peak must be removed from within ~ 150 pc at a (time-averaged) rate comparable to $\sim 1 M_{\odot} \text{ yr}^{-1}$ and transported out to a large radius without interfering with the X-ray appearance of NGC 4649 which resembles a traditional cooling flow. This mass outflow may occur in the bipolar jets observed in NGC 4649 and many other bright ellipticals. Alternatively, nuclear hot gas may become buoyant by intermittent local heating or by cosmic rays and flow out subsonically upstream in the cooling flow (e.g. Mathews & Brighenti 2008). If the buoyant gas density is only slightly less than that of the ambient gas, it may not significantly disturb the radial gas density and temperature profiles set by the inflowing gas. Alternatively, if the density of buoyant (or jet) gas were considerably lower, its X-ray emission would be less easily observed against the brighter emission from denser inflowing gas.

Studies of the evolution of hot gas in elliptical galaxies at UC Santa Cruz are supported by NSF and NASA grants for which we are very grateful.

REFERENCES

- Bell, E. F., et al. 2004, ApJ 608, 752
- Binney, J. & Tremaine, S. *Galactic Dynamics*, Princeton University Press, 1987
- Bregman, J. & Athey, A. E. 2003, Proc. of *The Riddle of Cooling Flows*, Charlottesville, VA May 31 - June 4, 2003, eds. T. Reiprich, J. empner & N. Soker, [http : //fuse.pha.jhu.edu/awf/fusepubs - /JHU/othr2004.html](http://fuse.pha.jhu.edu/awf/fusepubs-JHU/othr2004.html)
- Bregman J. N. & Parriott, J. R. 2009, ApJ 699, 923
- Arimoto, N., Matsushita, K., Ishimaru, Y., Ohashi, T., & Renzini, A. 1997, ApJ, 477, 128
- Baldi, A., Forman, W., Jones, C., Kraft, R., Nulsen, P., Churazov, E., David, L., & Giacintucci, S. 2009 (arXiv:094.2569)
- Brighenti, F. & Mathews, W. G. 2006, ApJ, 643, 120
- Brighenti, F. & Mathews, W. G. 2005, ApJ, 630, 864
- Brighenti, F. & Mathews, W. G. 2002, ApJ, 573, 442
- Brighenti, F. & Mathews, W. G. 2000, ApJ 539, 675
- Brighenti, F. & Mathews, W. G. 1999, ApJ, 527, L89
- Brighenti, F. & Mathews, W. G. 1997, ApJ, 486, L83
- Buote, D. A., Jeltema, T. E., Canizares, C. R., & Garmire, G.P. 2002, ApJ, 577, 183
- Caon, N., Macchetto, D., & Pastoriza, M. 2000, ApJS, 127, 39
- Cappellaro, E., Evans, R. & Turatto, M. 1999, A&A, 351, 459
- De Bruyne, et al. 2001, ApJ 546, 903
- Diehl, S. & Statler, T. S. 2008a, ApJ, 680, 897
- Diehl, S. & Statler, T. S. 2008b, ApJ, 687, 986
- Diehl, S. & Statler, T. S. 2007, ApJ, 668, 150
- Fang, Taotao, Humphrey, P. J. & Buote, D. A. 2008, ApJ (in press) (arXiv:0808.1106)
- Humphrey, P. J., Buote, D., Brighenti, F., Gebhardt, K. & Mathews, W. G. 2008, ApJ, 683, 161
- Humphrey, P. J. & Buote, D. 2006, ApJ, 639, 136
- Lauer, T. R. et al. 2005, AJ, 129, 2138
- Mathews, W. G. & Brighenti, F. 2008, ApJ (in print) (arXiv:0805.2441)
- Mathews, W. G. et al. 2006b, ApJ, 652, L17
- Mathews, W. G., Faltenbacher, A. & Brighenti, F. 2006a, ApJ 638, 659
- Mathews, W. G. & Brighenti, F. 2004, ApJ, 615, 745
- Mathews, W. G. & Brighenti, F. 2003b, ARA& 41, 191
- Mathews, W. G. & Brighenti, F. 2003a, ApJ 590, L5
- Mathews, W. G. & Brighenti, F. 1996, ApJ 470, 747
- Mathews, W. G., Brighenti, F. & Buote, D. A. 2004, ApJ 615, 662
- Mathews, W. G. 1990, ApJ, 354, 468
- Mathews, W. G. 1989, AJ, 97, 42
- McNamara, B. R. & Nulsen, P. E. J. 2007, Ann. Rev. Astron. & Astroph. 45, 117
- Parriott, J. R. & Bregman, J. N. 2008, ApJ, 681, 1215
- Peletier, R. F., et al. 1990, AJ 100, 1091
- Pinkney, J., Gebhardt, K., Aller, M., Bender, R., et al. 2003, ApJ 596, 903
- Scannapieco, E. & Brueggen, M. 2008, ApJ 686, 927
- Shurkin, K. et al., Dunn, R. J. H., Gentile, G., Taylor, G. B. & Allen, S. W. 2008, MNRAS 383, 923
- Stanger & Warwick 1986, MNRAS, 220, 363
- Sutherland, R. S., & Doptia, M. A. 1993, ApJS 88, 253
- Tem, P., Brighenti, F. & Mathews, W. G. 2007, ApJ, 666, 222
- Tonry, J. L., et al. 2001, ApJ, 546, 681
- van Dokkum, P. G. & Franx, M. 1995, AJ, 110, 2027
- Werner, N. et al. 2006, A&A, 459, 353
- Whittle, M. & Wilson, A. S. 2004, AJ, 127, 606
- Xu, H. et al., 2002, ApJ, 579, 600

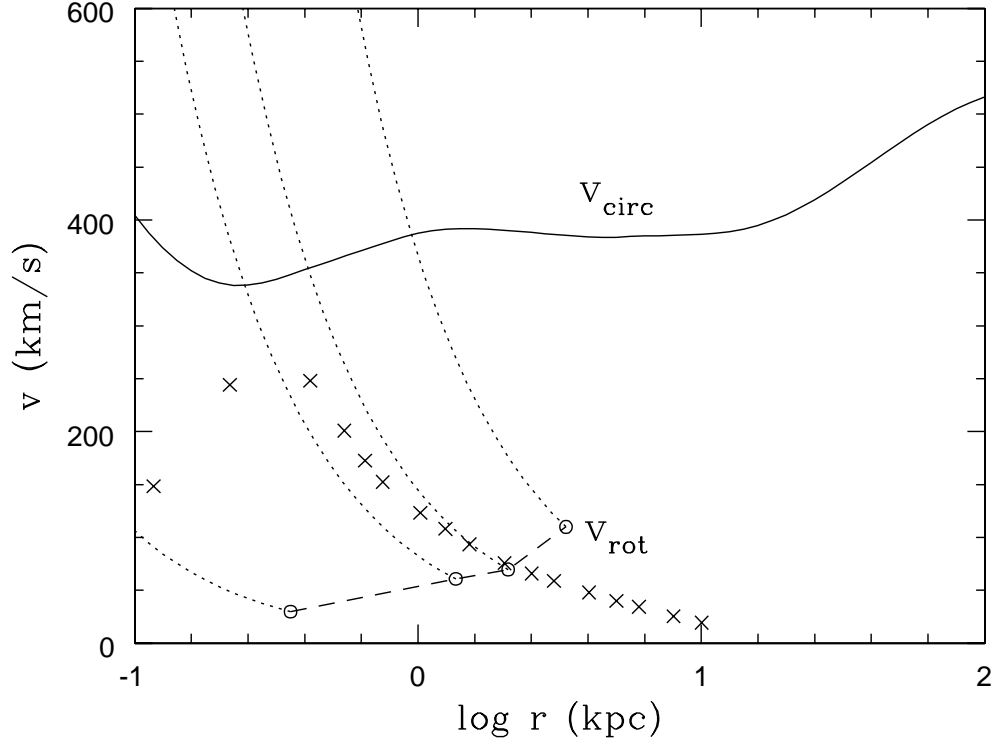


FIG. 1.— Comparison of circular velocity v_{circ} in NGC 4649 (*solid line*) with major axis stellar rotation v_{rot} (*dashed line*) from Pinkney et al. (2003). Dotted lines show trajectories of constant specific angular momentum. The crosses show the rotational velocity of the gas along the major axis as computed in our high resolution flow shown in Figure 8.

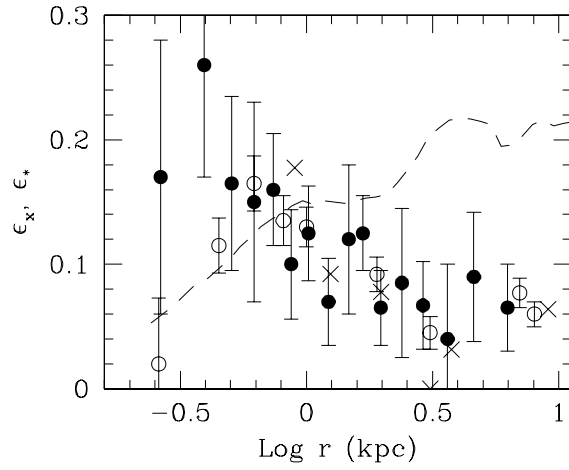


FIG. 2.— Ellipticity $\epsilon_X(r)$ of X-ray isophotes along major axis of NGC 4649 observed by Diehl & Statler (2007) (*filled circles*) and Humphrey et al. (*open circles*). Because of their deeper observations, the data from Humphrey et al. have smaller error bars. The *R*-band stellar ellipticity profile $\epsilon_*(r)$ is shown with a dashed line (Peletier et al. 1990). The crosses are approximate ellipticities of our high resolution rotating flow shown in Figure 8.

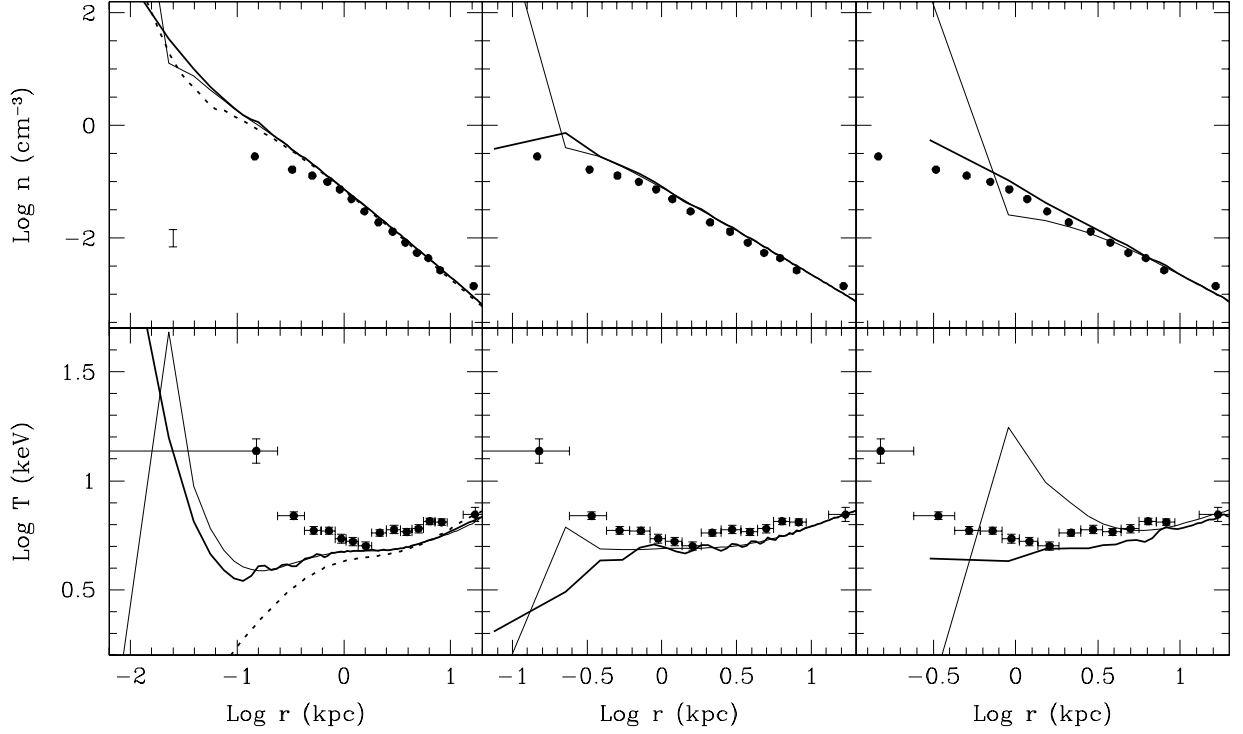


FIG. 3.— Electron density and temperature profiles in one-dimensional flows for NGC 4649 after 6 Gyrs compared with observations of Humphrey et al. (2008). A representative mean error bar for the density observations is shown in the upper left panel. Calculations are repeated at three different grid resolutions with central zones of size $\Delta r = 15, 150$ and 600 pc respectively from left to right. Each calculation is performed with no removal of cooled gas ($q = 0$; *thin lines*) and continuous removal ($q = q(T)$; *thick lines*). For comparison the heavy dotted lines in the left panels show high resolution density and temperature profiles with $q = q(T)$ when the central black hole is removed. The density inversion within 30 pc in the central panel is a transient feature associated with this mass removal.

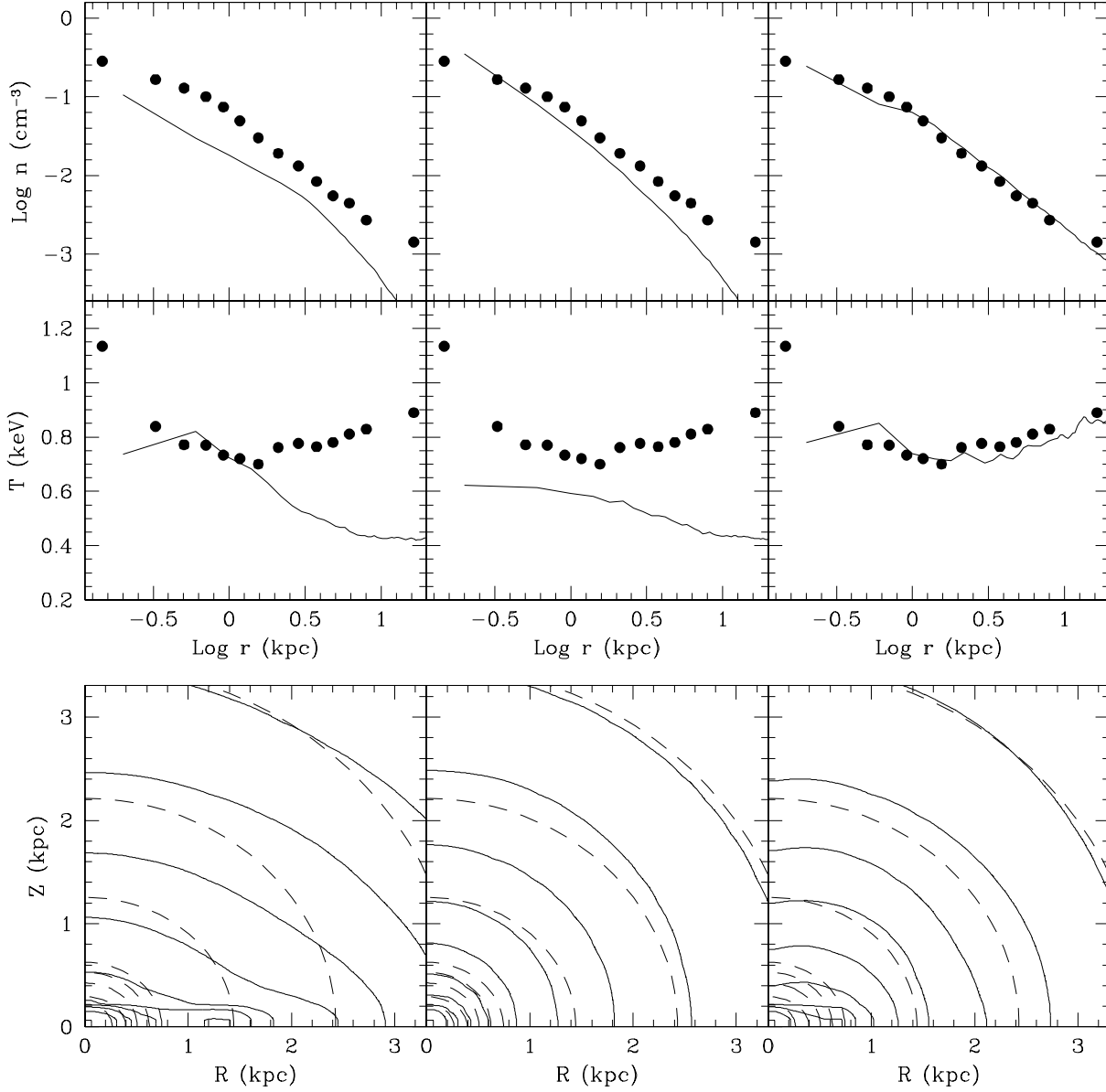


FIG. 4.— Two dimensional rotating flows for NGC 4649 computed after 6 Gyrs in three columns of panels: *Left panels*: flow without turbulent viscosity or circumgalactic gas; *Central panels*: flow with turbulent viscosity but no circumgalactic gas; *Right panels*: flow without turbulent viscosity but with circumgalactic gas. The upper two panels compare computed, azimuthally averaged gas temperature and density with observations from Humphrey et al. (2008). Panels at the bottom compare the computed bolometric X-ray isophotes with the observed X-ray ellipticity $\epsilon_X(r)$. (dashed lines).

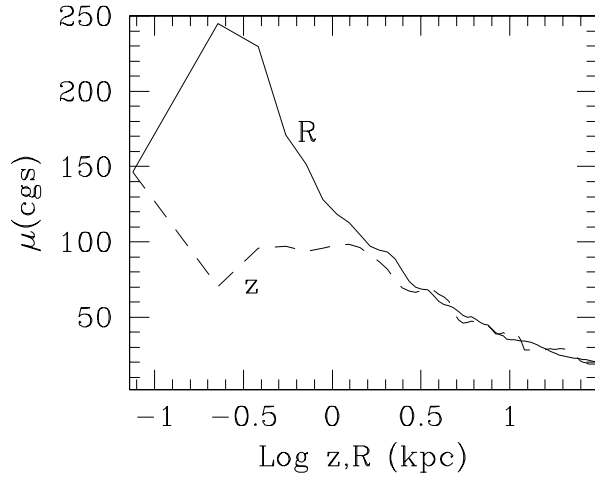


FIG. 5.— Turbulent viscosity profiles after 6 Gyrs along the z -axis ($\mu(0, z)$; *dashed line*) and along the R -axis ($\mu(R, 0)$; *solid line*) both using reference model parameters ($v_t = 50 \text{ km s}^{-1}$ and $f = 0.05$). The viscosity is evaluated at the center of each computational zone and therefore must agree for the innermost zone.

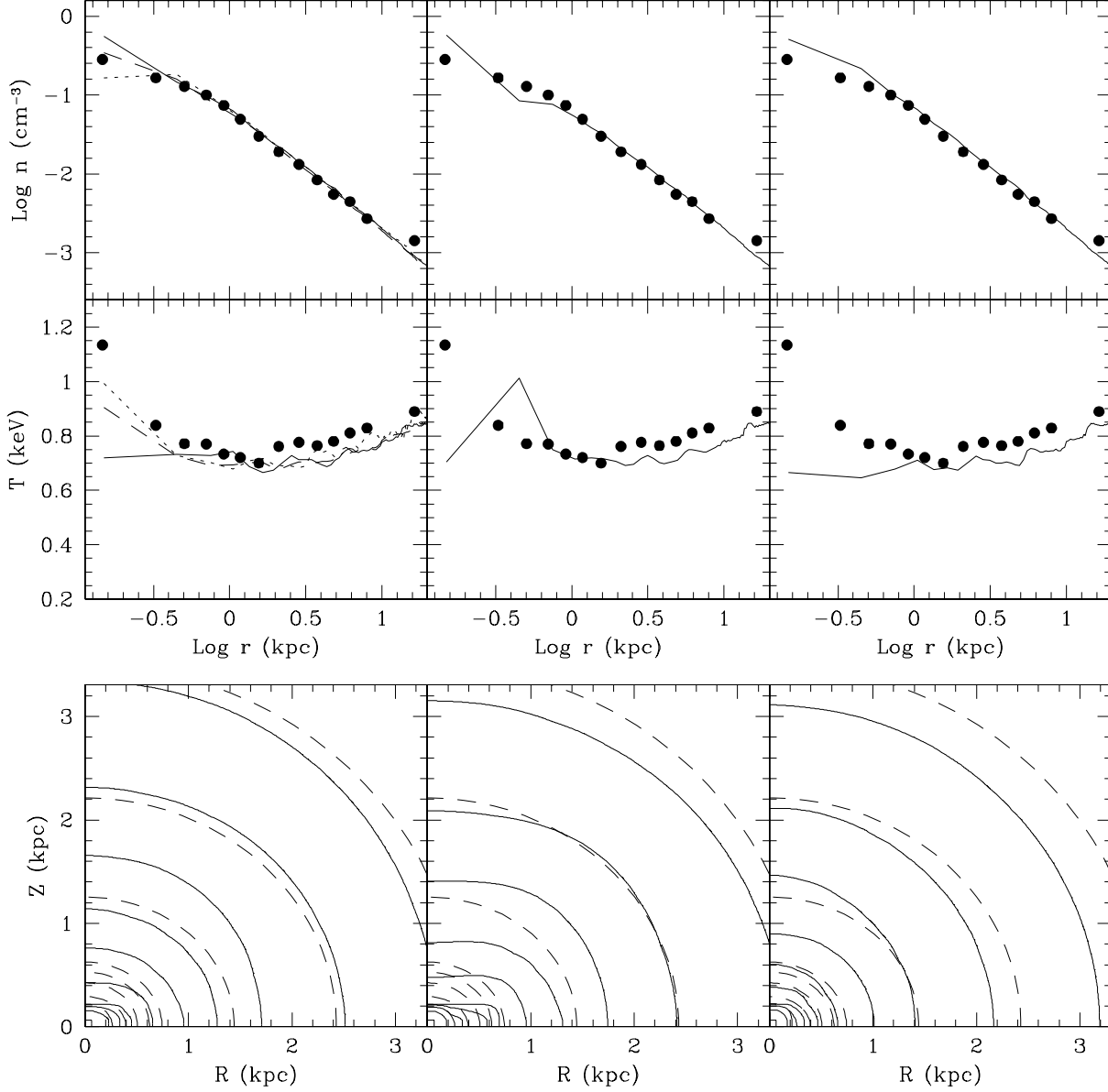


FIG. 6.— Two dimensional flows for NGC 4649 computed after 6 Gyrs in three columns of panels: *Left panels:* reference flow with turbulent viscosity parameters $v_t = 50 \text{ km s}^{-1}$ and $f = 0.05$. The flow oscillates unrealistically near the center as gas is removed rather abruptly due to cooling, even at relatively high spatial resolution. The three curves show typical excursions at 4 Gyrs (*dotted lines*), 6 Gyrs (*solid lines*), and 8 Gyrs (*dashed lines*); *Central panels:* flow with turbulent viscosity parameters $v_t = 25 \text{ km s}^{-1}$ and $f = 0.025$; *Right panels:* flow with turbulent viscosity parameters $v_t = 50 \text{ km s}^{-1}$ and $f = 0.1$. All flows contain circumgalactic gas. The upper two panels compare computed, azimuthally averaged gas temperature and density with observations from Humphrey et al. (2008). Panels at the bottom compare the computed bolometric X-ray isophotes with the observed X-ray ellipticity. (*dashed lines*).

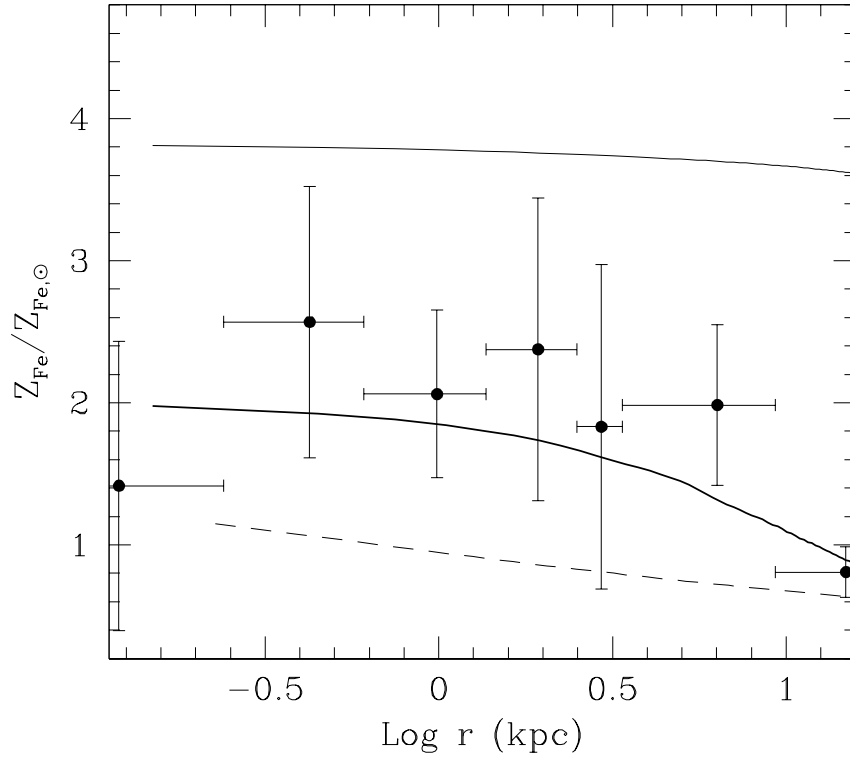


FIG. 7.— Plot of azimuthally averaged gas phase (*heavy solid line*) and stellar (*dashed line*) iron abundance profiles after 6 Gyrs for the reference model with circumgalactic gas having initial abundance $z_{cgg} = 0.6z_{\odot}$. The light solid line shows the unrealistically high abundances that result in the reference flow when circumgalactic gas is absent. The hot gas iron abundance observed in NGC 4649 shown with error bars are based on data discussed in Humphrey et al. (2007).

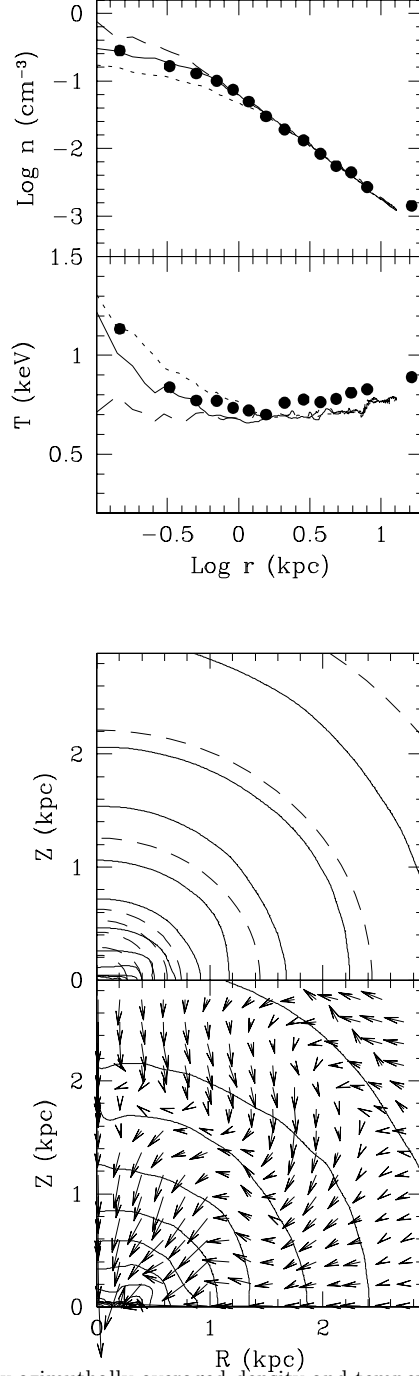


FIG. 8.— The top two panels show azimuthally-averaged density and temperature profiles for the the reference flow ($v_t = 50 \text{ km s}^{-1}$ and $f = 0.05$) computed at high resolution (*solid lines*). The two additional high resolution flows are done with different viscosity parameters: $v_t = 25 \text{ km s}^{-1}$ and $f = 0.025$, (*dotted lines*), and $v_t = 50 \text{ km s}^{-1}$ and $f = 0.1$, (*dashed lines*). The third panel down compares the computed bolometric X-ray contours (*solid lines*) with observations (*dashed lines*). The bottom panel shows the velocity field in the hot gas. The velocity in km s^{-1} can be found by multiplying the vector length in kpc by 75.

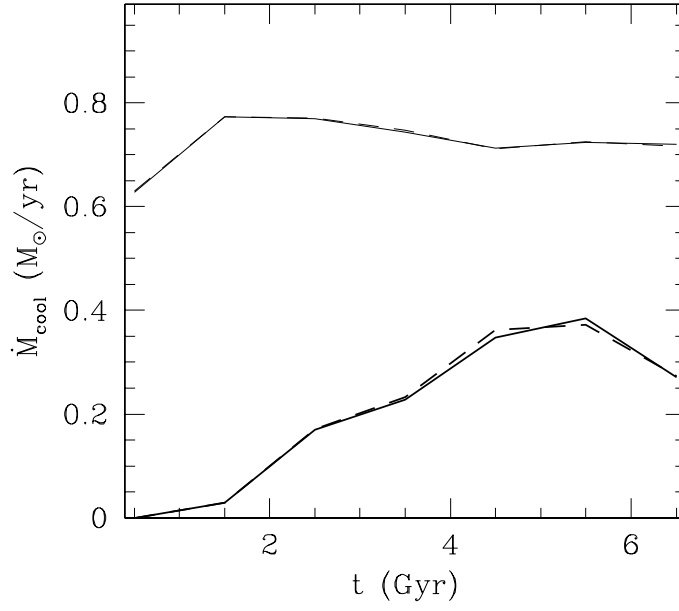


FIG. 9.— Rate that gas would cool near the center of NGC 4649. *Heavy lines:* Flows without circumgalactic gas without viscosity (*dashed heavy line*) and with viscosity parameters $v_t = 50 \text{ km s}^{-1}$ and $f = 0.1$ (*solid heavy line*). *Light lines:* Flows with circumgalactic gas without viscosity (*dashed light line*) and with viscosity parameters for the reference model $v_t = 50 \text{ km s}^{-1}$ and $f = 0.05$ (*solid light line*). These two cooling rates are nearly identical.